Available online at www.sciencedirect.com
ScienceDirect
International Journal of Heat and Mass Transfer 50 (2007) 3788–3798
International Journal of HEAT and MASS TRANSFER
www.elsevier.com/locate/ijhmt

A numerical study of momentum and forced convection heat transfer around two tandem circular cylinders at low Reynolds numbers. Part I: Momentum transfer

Gheorghe Juncu *

Politehnica University Bucharest, Catedra Inginerie Chimica, Polizu 1, 78126 Bucharest, Romania

Received 13 July 2006
Available online 20 April 2007

Abstract

This work presents a computational study of the steady, axisymmetric, viscous flow around two circular cylinders in tandem. The vorticity–stream function formulation of the Navier–Stokes equations was chosen. Numerical solutions have been obtained in bipolar cylindrical coordinates. A compact, high-order, finite difference method was used to discretize the model equations. Iterative algorithms were tested to solve the discrete equations. Different cylinders spacing and sizes were considered for the upstream cylinder Reynolds number up to 30. Vorticity and pressure distributions on the cylinders surfaces and drag coefficients are presented and compared with those calculated for an isolated cylinder.

Keywords: Two circular cylinders; Tandem arrangement; Steady laminar flow; Bipolar cylindrical coordinates; Compact finite difference scheme; Iterative methods

1. Introduction

The interaction of the flow over two cylinders is a topic of prime scientific interest with many engineering and real life applications. Significant research has been done, both experimentally and numerically, for the understanding of this problem [1,2]. The arrangement of the cylinders versus the flow direction of the free stream is the classification criterion usually used in the analysis of the hydrodynamic interaction between two cylinders. The arrangement of the cylinders with respect to the free stream flow direction can be

- tandem (or in-line) – the free stream flow direction is parallel with the line of the centers of the cylinders;
- transverse (or side-by-side) – the free stream flow direction is perpendicular to the line of the cylinders centers;
- staggered.

The flow past two cylinders in tandem was analysed numerically in [3–15]. Li et al. [3] used the velocity–pressure formulation to solve the unsteady, 2D, incompressible Navier–Stokes equations. The pressure distribution around both cylinders and their vortex shedding frequencies as a function of cylinder interval were determined for $Re = 100$. The random vortex method was used to investigate the flow around two cylinders in transverse and tandem arrangements in [4]. The computations were carried out at a Reynolds number of 200. Mittal et al. [5] used a stabilized finite element formulation on a Cartesian grid to study incompressible flows past a pair of equal-sized cylinders at Reynolds numbers 100 and 1000. Computations are carried out for three sets of cylinder arrangements, two in tandem and one staggered. A spectral element method on a Cartesian grid was employed in [6] to investigate the interference effects when two cylinders or two spheres are placed in series or parallel in a low Reynolds number flow. For two cylinders in-line, Cheung et al. [6] analysed only the case of cylinders with the same diameters

* Tel./fax: +40 21 345 05 96.
E-mail addresses: juncugh@netscape.net, juncu@easynet.ro

0017-9310/$ - see front matter © 2007 Elsevier Ltd. All rights reserved.
doi:10.1016/j.ijheatmasstransfer.2007.02.020

Nomenclature

c	characteristic length, bipolar cylindrical coordinate system
C_D	drag coefficient
C_P	pressure coefficient
d	diameter of the cylinder
L	distance from the center of the cylinder to the origin of the coordinate system
Re	Reynolds number based on diameter of the upstream cylinder, $Re = U_\infty d_1/\nu$
U_∞	free stream velocity
x	streamwise (horizontal) coordinate, Cartesian coordinate system
y	transverse (vertical) coordinate, Cartesian coordinate system

Greek symbols

η	bipolar cylindrical coordinate
λ	drag ratio
μ	dynamic viscosity
ν	kinematic viscosity
ρ	density
ω	vorticity
ξ	bipolar cylindrical coordinate
ψ	stream function

Subscripts

F	friction
P	pressure
s	surface of the cylinder
1	refers to the upstream cylinder
2	refers to the downstream cylinder

at $Re = 1$. The results are depicted in terms of the drag ratio.

The shedding of vortices and flow interference between two circular cylinders in tandem and side-by-side arrangements were investigated numerically for a Reynolds number varying from 100 to 200 by Meneghini et al. [7]. A fractional step method was used in [7] to solve the unsteady, 2D, Navier–Stokes equations. The flow-induced oscillations of a pair of equal-sized cylinders in tandem and staggered arrangement placed in uniform incompressible flow for Reynolds number 100 are studied by Mittal and Kumar [8]. Flows over two tandem cylinders were analysed numerically using a new collocated unstructured computational fluid dynamics code (CUCFD) in [9,10]. The mean and fluctuating surface pressure distribution, lift and drag coefficients were calculated for centre-to-centre cylinder spacing between 2 and 10 diameters at a Reynolds number equal to 100. A comprehensive numerical investigation of incompressible flow about fixed cylinders pairs in tandem, side-by-side and staggered arrangements at Reynolds numbers of 80 and 1000 can be viewed in [11]. A second order streamline upwind Petrov–Galerkin projection scheme was used along with routines for interactive steering and dynamic meshing. Khorrami et al. [12] solved the two-dimensional, unsteady Reynolds Averaged Navier–Stokes equations with a two-equation turbulence model, at a Reynolds number of 0.166×10^6 and a Mach number of 0.166. This setup is viewed to be a representative for several component-level flow interactions that occur when air flows over the main landing gear of large civil transports. The instability and transition of flow past two circular cylinders arranged in tandem were investigated numerically by Mizushima and Suehiro [13]. It was found that the transition of the flow from a steady state to an oscillatory state occurs due to a supercritical or subcritical Hopf bifurcation depending upon the gap spacing. For the upstream cylinder Re number equal to 2, the Navier–Stokes equations in the vorticity–stream function formulation in bipolar cylindrical coordinate system were solved numerically in [14]. Different cylinders spacing and sizes were considered. Two- and three-dimensional simulations of the flow around pairs of rigid and immovable circular cylinders in tandem were made by Carmo [15]. The centre-to-centre distance varies between 1.5 and 8 diameters and the Re range goes from 160 to 320.

The flow past two cylinders in tandem is used as a test problem for new computational methods in [16–19]. Young et al. [16] proposed a three-step FEM-BEM computational technique to simulate high-Reynolds number flow past circular cylinders in 2D incompressible viscous flows. Guermond and Lu [17] introduced a domain decomposition method for simulating 2D external, incompressible viscous flows. Steady state and time dependent vortex shedding flows were computed using a second order time stepping numerical scheme within a cell boundary element method by Farrant et al. [18]. Russell and Wang [19] used an underlying regular Cartesian grid to solve 2D incompressible viscous flows around multiple moving objects.

The finite difference high-order compact schemes have attracted a considerable amount of attention in the area of viscous incompressible flow calculations [20–28]. In comparison with other finite difference schemes, the high-order compact schemes offer three attractive features: (1) high order accuracy; (2) unconditional stability; and (3) relatively easy boundary treatment. These schemes also compare well with spectral methods. They have the advantage of being simple, robust, efficient and much more stable (we should mention that the Chebyshev methods resolve

boundary layers better than finite difference on uniform grids). However, the computational advantages of these schemes have not been exhaustively explored. The driven cavity is the only case of 2D, steady, incompressible Navier–Stokes equations worked. Complex problems were solved in an unsteady formulation in [29,30].

This paper has a double aim. First, we wish to complete the analysis of the flow past two cylinders in tandem at low Reynolds numbers. Different cylinders spacing and sizes were considered for the upstream cylinder Reynolds number up to 30. Second, we wish to test the abilities of the combination of high-order compact schemes–iterative methods in solving the Navier–Stokes equations in stream function–vorticity formulation in bipolar cylindrical coordinate system.

The outline of this paper is as follows. Section 2 presents the mathematical model of the 2D steady, incompressible flow past two cylinders in tandem. The numerical methods employed are described in Section 3. In Section 4 we illustrate the use of these methods by providing the numerical experiments made. Section 5 is devoted to some concluding remarks.

2. Statement of the problem

Let us consider two infinitely long cylinders of diameters d_i, $i = 1, 2$, placed in a horizontal flow, parallel with their line of centers, of an incompressible fluid having free stream velocity U_∞ (as illustrated in Fig. 1). The diameters of the cylinders are assumed considerably higher than the molecular mean free path of the surrounding fluid. The fluid is homogeneous, Newtonian and the flow is steady and laminar. The density ρ and viscosity μ of the fluid are considered constant. Oscillations and rotation of the cylinders do not occur during the flow.

Let a system of Cartesian coordinates (x, y, z) be chosen so that the centres of the cylinders lie along the x-axis (see also Fig. 1). The cylinders being considered infinitely long, the flow does not depend on z-coordinate. Also, for low Reynolds numbers, we can consider the flow symmetric versus the y-axis.

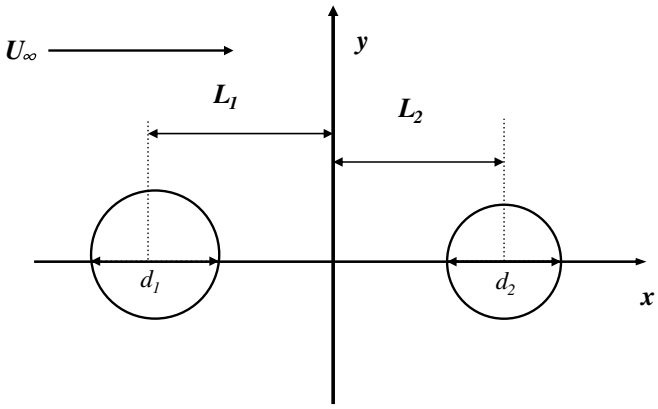

Fig. 1. Schematic of the problem.

Based on the previous assumptions, in Cartesian coordinates, the stream function (ψ) – vorticity (ω) formulation of the steady, two-dimensional, incompressible viscous flow equations is given by

$$\frac{\partial\psi}{\partial y}\frac{\partial\omega}{\partial x} - \frac{\partial\psi}{\partial x}\frac{\partial\omega}{\partial y} = \nu\left(\frac{\partial^2\omega}{\partial x^2} + \frac{\partial^2\omega}{\partial y^2}\right) \tag{1a}$$

$$\frac{\partial^2\psi}{\partial x^2} + \frac{\partial^2\psi}{\partial y^2} = \omega \tag{1b}$$

where ν is the kinematic viscosity of the fluid.

The most convenient coordinate system for a pair of cylinders in tandem is the orthogonal bipolar cylindrical coordinate system. The bipolar cylindrical coordinate system is defined by [31]

$$x = \frac{c\sin\xi}{\cosh\eta - \cos\xi}; \quad y = \frac{c\sinh\eta}{\cosh\eta - \cos\xi}; \quad z = z$$

where $c > 0$ is a characteristic length. This transformation maps the upper half of the (x, y) – plane (from which the domain occupied by the cylinders is excluded) into the rectangle $\eta_1 \leqslant \eta \leqslant \eta_2,\ 0 \leqslant \xi \leqslant \pi$ ($\eta_1 < 0,\ \eta_2 > 0$). The surfaces of the cylinders are located at $\eta = \eta_1$ and $\eta = \eta_2$. The relations between η_i, the diameters of the cylinders d_i and the distances L_i of their centers from the origin of the coordinates system are

$$\frac{d_i}{2} = \frac{c}{\sinh|\eta_i|}; \quad L_i = c\coth|\eta_i|, \quad i = 1, 2$$

If an orthogonal curvilinear coordinate system is used, the Navier–Stokes equations in the stream-function – vorticity formulation can be transformed according to the relations $\xi = \xi(x, y)$ and $\eta = \eta(x, y)$ and can be rewritten as [32]

$$\left(\frac{\partial\psi}{\partial\eta}\frac{\partial\omega}{\partial\xi} - \frac{\partial\psi}{\partial\xi}\frac{\partial\omega}{\partial\eta}\right)\Big/ J = \nu\left(\alpha\frac{\partial^2\omega}{\partial\xi^2} - 2\beta\frac{\partial^2\omega}{\partial\xi\partial\eta} + \gamma\frac{\partial^2\omega}{\partial\eta^2}\right)\Big/ J^2 \tag{2a}$$

$$\alpha\frac{\partial^2\psi}{\partial\xi^2} - 2\beta\frac{\partial^2\psi}{\partial\xi\partial\eta} + \gamma\frac{\partial^2\psi}{\partial\eta^2} = \omega J^2 \tag{2b}$$

where

$$\alpha = \left(\frac{\partial x}{\partial\eta}\right)^2 + \left(\frac{\partial y}{\partial\eta}\right)^2, \quad \beta = \frac{\partial x}{\partial\xi}\frac{\partial x}{\partial\eta} + \frac{\partial y}{\partial\eta}\frac{\partial y}{\partial\xi},$$
$$\gamma = \left(\frac{\partial x}{\partial\xi}\right)^2 + \left(\frac{\partial y}{\partial\xi}\right)^2, \quad J = \frac{\partial x}{\partial\xi}\frac{\partial y}{\partial\eta} - \frac{\partial x}{\partial\eta}\frac{\partial y}{\partial\xi}.$$

For the bipolar cylindrical coordinate system, α, β, γ and J are given by

$$\alpha = \gamma = J = \frac{c^2}{(\cosh\eta - \cos\xi)^2}, \quad \beta = 0.$$

The governing equations can be non-dimensionalized by using the radius of the leading cylinder $d_1/2$ for length, U_∞ for velocity, $U_\infty d_1/2$ for stream function and $2U_\infty/d_1$

for vorticity. Also, it is convenient numerically to work with the deviation from the uniform flow ψ^*,

$$\psi^* = \psi - \frac{\bar{c}\sin\xi}{\cosh\eta - \cos\xi}; \quad \bar{c} = \frac{2c}{d_1}.$$

After α, β, γ and J are expressed explicitly in (2), the dimensionless Navier–Stokes equations are

$$\frac{(\cosh\eta - \cos\xi)^2}{\bar{c}^2}\left(\frac{\partial^2\psi^*}{\partial\eta^2} + \frac{\partial^2\psi^*}{\partial\xi^2}\right) = \omega \tag{3a}$$

$$\left[\frac{\partial\omega}{\partial\xi}\left(\frac{\partial\psi^*}{\partial\eta} - \frac{\bar{c}\sin\xi\sinh\eta}{(\cosh\eta - \cos\xi)^2}\right) - \frac{\partial\omega}{\partial\eta}\left(\frac{\partial\psi^*}{\partial\xi} + \frac{\bar{c}(\cosh\eta\cos\xi - 1)}{(\cosh\eta - \cos\xi)^2}\right)\right] = \frac{2}{Re}\left(\frac{\partial^2\omega}{\partial\eta^2} + \frac{\partial^2\omega}{\partial\xi^2}\right) \tag{3b}$$

where the Reynolds number Re, based on the leading cylinder diameter d_1, is

$$Re = U_\infty d_1/\nu.$$

The boundary conditions for the dimensionless streamfunction and vorticity are

– cylinders surfaces ($\eta = \eta_i, i = 1, 2$)

$$\psi^* = -\bar{c}\sin\xi/(\cosh\eta - \cos\xi) \tag{4a}$$

– free stream ($\eta \to 0, \xi \to 0$)

$$\psi^* \to 0, \omega \to 0 \tag{4b}$$

– symmetry axis ($\xi = 0$ and $\eta \neq 0, \xi = \pi$)

$$\psi^* = \omega = 0 \tag{4c}$$

The pressure coefficients, $C_{P,i}(\xi)$, on the cylinders surfaces and the drag coefficients, $C_{D,i}$, are computed with the relations [32],

$$C_{P,i}(\xi) = P(\xi) - P(\xi_{ref}) = \frac{2}{Re}\int_{\xi_{ref}}^{\xi}\left.\frac{\partial\omega}{\partial\eta}\right|_{\eta=\eta_i} d\xi \quad i = 1, 2 \tag{5}$$

$$C_{D,i} = \frac{d_1}{d_i}\left[2\int_{\xi_{min}}^{\xi_{max}}\frac{\partial\bar{y}}{\partial\xi}C_P(\xi)d\xi + \frac{4}{Re}\int_{\xi_{min}}^{\xi_{max}}\frac{\partial\bar{x}}{\partial\xi}\omega d\xi\right] \quad i = 1, 2 \tag{6}$$

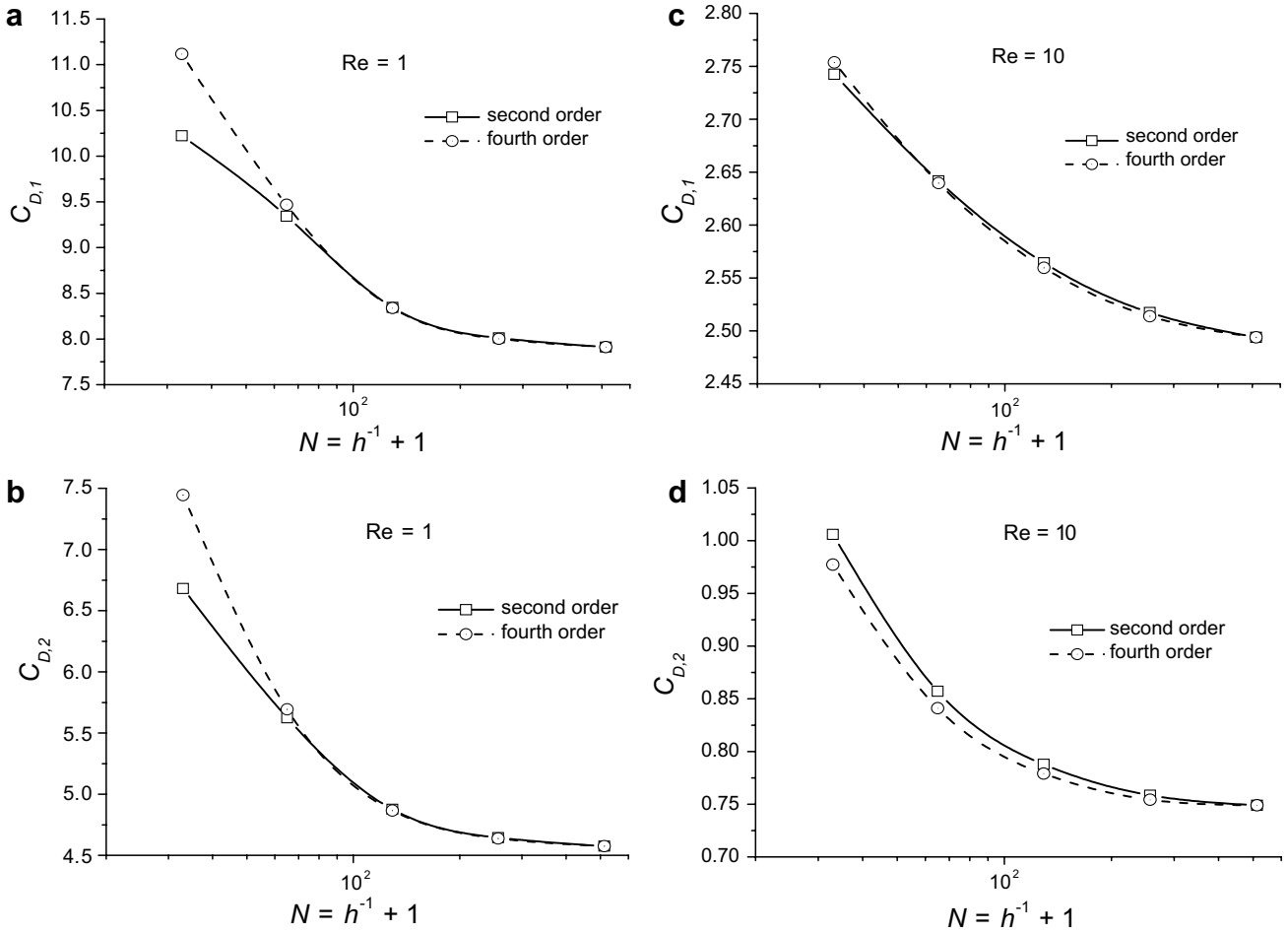

Fig. 2. Influence of the numerical approximation of the pseudo-velocities on the drag coefficients for different meshes; $d_1 = d_2 = d$ and $2L/d = 2$; (a) upstream cylinder at $Re = 1$; (b) downstream cylinder at $Re = 1$; (c) upstream cylinder at $Re = 10$; (d) downstream cylinder at $Re = 10$.

where

$$\bar{x} = \frac{2x}{d_1}, \quad \bar{y} = \frac{2y}{d_1}.$$

The two integrals in (6) are referred as the pressure and friction drag coefficients and are denoted $C_{DP,i}$ and $C_{DF,i}$, respectively. In relations (5) and (6), for both cylinders, $\xi_{ref} = \xi_{min} = 0$ and $\xi_{max} = \pi$. For this reason, the sign "–" should be considered for the integrals in (6), when the calculations are carried out for the trailing cylinder.

Table 1
Drag coefficients for the isolated cylinder and tandem cylinders at $d_1 = d_2 = d$ and $2L/d = 2$

Re	Isolated cylinder			Tandem cylinders					
	C_{DP}	C_{DF}	C_D	C_{DP1}	C_{DF1}	C_{D1}	C_{DP2}	C_{DF2}	C_{D2}
1	5.225	5.118	10.343	3.915	3.990	7.905	2.10	2.482	4.582
2	3.396	3.233	6.629	2.751	2.682	5.433	1.202	1.442	2.644
5	2.074	1.819	3.893	1.819	1.617	3.436	0.573	0.727	1.30
10	1.526	1.196	2.722	1.404	1.106	2.510	0.319	0.425	0.744
15	1.308	0.936	2.244	1.225	0.875	2.10	0.220	0.307	0.527
20	1.195	0.795	1.990	1.135	0.750	1.885	0.160	0.240	0.40
25	1.103	0.684	1.787	1.077	0.659	1.736	0.117	0.194	0.311
30	1.044	0.611	1.655	1.038	0.594	1.632	0.085	0.162	0.247

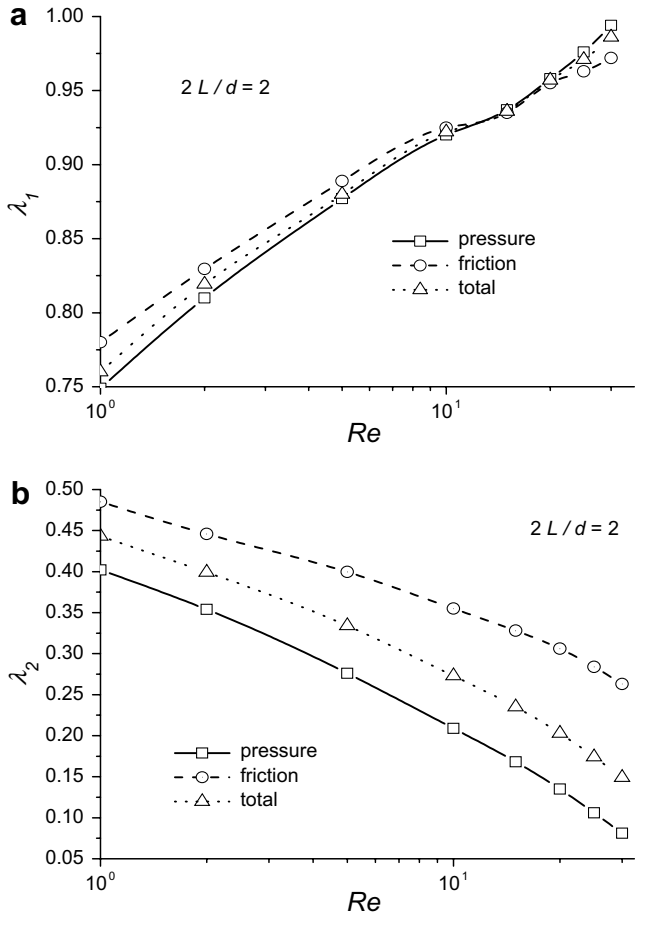

Fig. 3. Influence of the *Re* number on the drag ratio for $d_1 = d_2 = d$ and $2L/d = 2$; (a) upstream cylinder; (b) downstream cylinder.

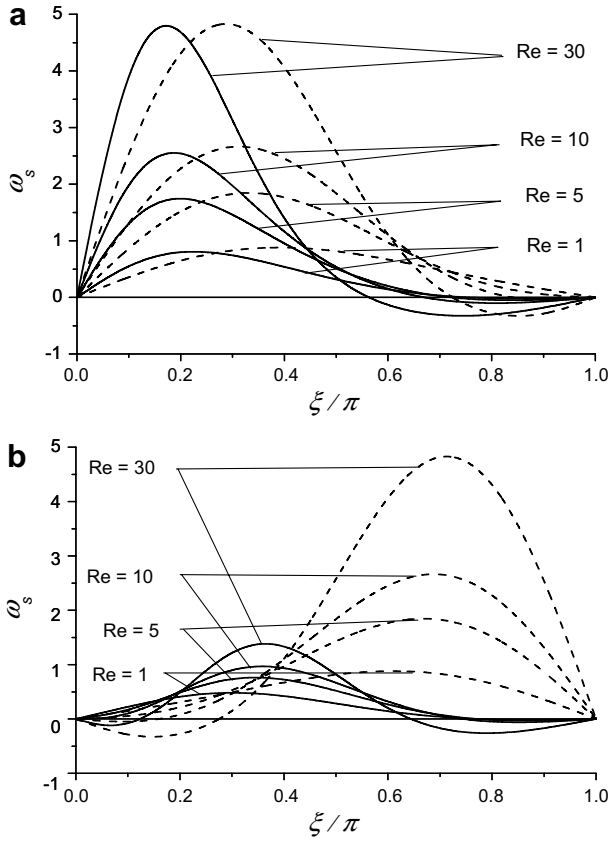

Fig. 4. The vorticity distribution over the body surface for $d_1 = d_2 = d$, $2L/d = 2$ and different *Re* values; —- tandem cylinder; - - - isolated cylinder; (a) upstream cylinder; (b) downstream cylinder.

3. Solution procedure

The Navier–Stokes equations were solved numerically. The two-dimensional domain $(\eta_1, \eta_2) \times (0, \pi)$ was transformed into the unit square. In the unit square, Eq. (3) read as

$$\frac{(\cosh\eta - \cos\pi\bar{\xi})^2}{\bar{c}^2}\left(\frac{1}{\eta_{21}^2}\frac{\partial^2\psi^*}{\partial\bar{\eta}^2} + \frac{1}{\pi^2}\frac{\partial^2\psi^*}{\partial\bar{\xi}^2}\right) = \omega \tag{7a}$$

$$\left[\frac{\partial\omega}{\pi\partial\bar{\xi}}\left(\frac{\partial\psi^*}{\eta_{21}\partial\bar{\eta}} - \frac{\bar{c}\sin\pi\bar{\xi}\sinh\eta}{(\cosh\eta - \cos\pi\bar{\xi})^2}\right) - \frac{\partial\omega}{\eta_{21}\partial\bar{\eta}}\left(\frac{\partial\psi^*}{\pi\partial\bar{\xi}} + \frac{\bar{c}(\cosh\eta\cos\pi\bar{\xi} - 1)}{(\cosh\eta - \cos\pi\bar{\xi})^2}\right)\right] = \frac{2}{Re}\left(\frac{1}{\eta_{21}}\frac{\partial^2\omega}{\partial\bar{\eta}^2} + \frac{1}{\pi^2}\frac{\partial^2\omega}{\partial\bar{\xi}^2}\right) \tag{7b}$$

where $\bar{\eta} = \frac{\eta - \eta_1}{\eta_{21}}$, $\eta_{21} = \eta_2 - \eta_1$ and $\bar{\xi} = \frac{\xi}{\pi}$.

Eq. (7) were discretized with a high order compact (HOC) finite difference scheme. For a general convection–diffusion equation, the derivation of the HOC scheme is well presented in [33–39]. Two mechanisms were used: collocation [33–35] and Taylor series expansion [36–39]. We did not consider it necessary to reproduce these calculations here. The vorticity equation (7b) is similar to that obtained in Cartesian coordinates. Discrete HOC approximations for (7b) can be easily deduced from those pre-

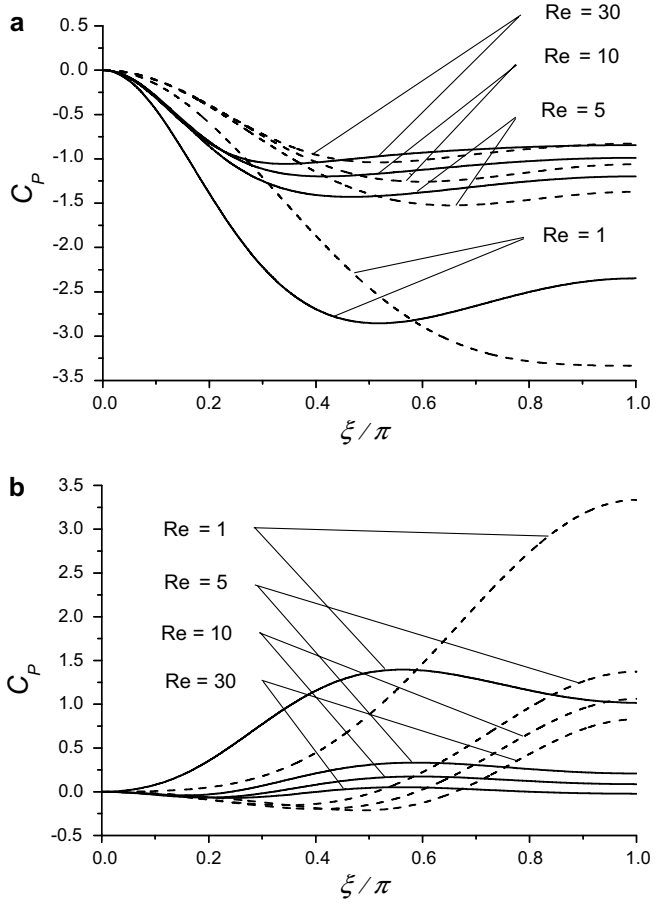

Fig. 5. Pressure coefficient over the cylinders surfaces for $d_1 = d_2 = d$, $2L/d = 2$ and different Re values; —- tandem cylinder; - - - isolated cylinder; (a) upstream cylinder; (b) downstream cylinder.

sented in [20–26]. We will present in detail the discrete approximation of the stream function Eq. (7a).

For a uniform grid, we number the grid points (ξ,η), $(\xi+h,\eta)$, $(\xi,\eta+h)$, $(\xi-h,\eta)$, $(\xi,\eta-h)$, $(\xi+h,\eta+h)$, $(\xi-h,\eta+h)$, $(\xi-h,\eta-h)$ and $(\xi+h,\eta-h)$ as M, E, N, W, S, NE, NW, SW and SE, respectively, where h is the grid size. By [35], the HOC scheme for (7a) is

$$\begin{bmatrix} C_{NW} & C_N & C_{NE} \\ C_W & -C_M & C_E \\ C_{SW} & C_S & C_{SE} \end{bmatrix} \psi^* = \frac{h^2}{2}\begin{bmatrix} 0 & 1 & 0 \\ 1 & 8 & 1 \\ 0 & 1 & 0 \end{bmatrix}\omega + h^3\left[\frac{\pi \sin\xi}{\cosh\eta - \cos\xi}(\omega_W - \omega_E) + \frac{\eta_{21}\sinh\eta}{\cosh\eta - \cos\xi}(\omega_S - \omega_N)\right]$$

where

$$C_E = C_W = \frac{(\cosh\eta - \cos\xi)^2}{\bar{c}^2}\left(\frac{5}{\pi^2} - \frac{1}{\eta_{21}^2}\right) - \frac{2h^2}{\pi^2\bar{c}^2}\left[\pi^2\sin^2\xi + \eta_{21}^2\sinh^2\eta + \frac{\eta_{21}^2 - \pi^2}{2}(\cosh\eta\cos\xi - 1)\right]$$

Table 2
Values of the drag ratio for $d_1/d_2 = 1$

λ	Re	$2L/d$			
		2	3	4	5
λ_1	1	0.764	0.804	0.846	0.884
λ_2		0.443	0.47	0.498	0.53
λ_1	10	0.922	0.926	0.933	0.95
λ_2		0.273	0.323	0.364	0.408

$$C_N = C_S = \frac{(\cosh\eta - \cos\xi)^2}{\bar{c}^2}\left(\frac{5}{\eta_{21}^2} - \frac{1}{\pi^2}\right) - \frac{2h^2}{\eta_{21}^2\bar{c}^2}\left[\pi^2\sin^2\xi + \eta_{21}^2\sinh^2\eta + \frac{\eta_{21}^2 - \pi^2}{2}(\cosh\eta\cos\xi - 1)\right]$$

$$C_{NE} = C_{NW} = C_{SE} = C_{SW} = \frac{(\cosh\eta - \cos\xi)^2}{2\bar{c}^2}\left(\frac{1}{\pi^2} + \frac{1}{\eta_{21}^2}\right)$$

$$C_M = C_M + C_S + C_E + C_W + C_{NE} + C_{NW} + C_{SE} + C_{SW}.$$

When HOC schemes are applied to the Navier–Stokes equations in stream function – vorticity formulation, the

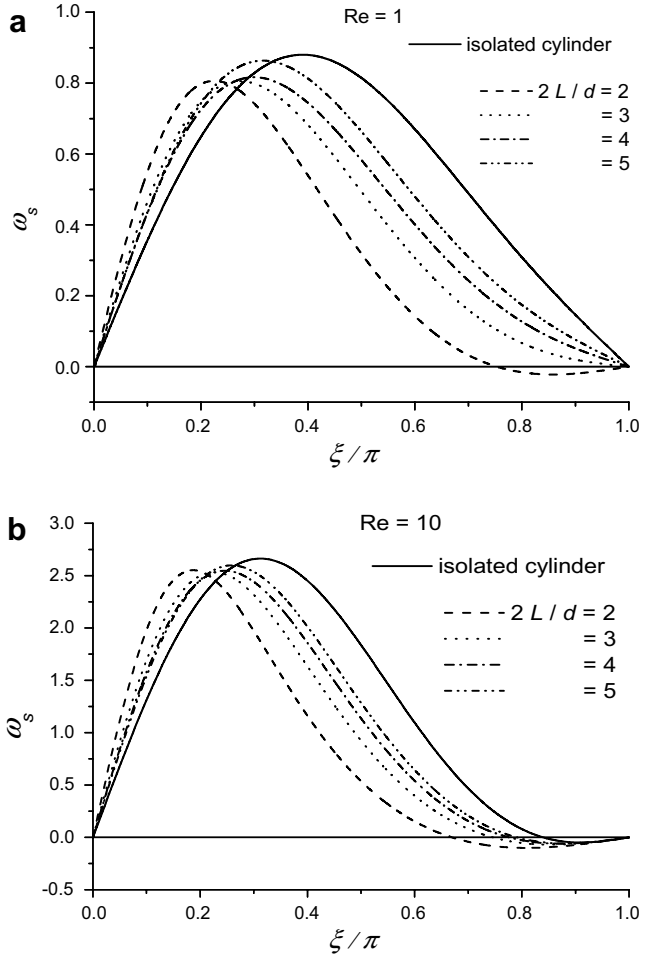

Fig. 6. The influence of the gap between cylinders on the surface vorticity of the leading cylinder; $d_1 = d_2 = d$; (a) $Re = 1$; (b) $Re = 10$.

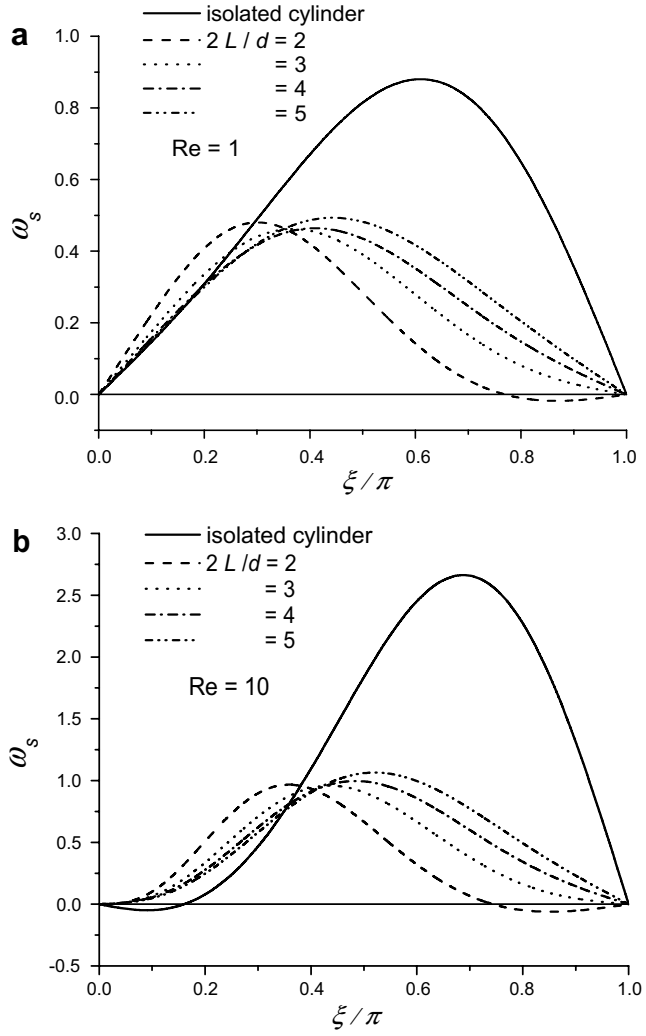

Fig. 7. The influence of the gap between cylinders on the surface vorticity of the trailing cylinder; $d_1 = d_2 = d$; (a) $Re = 1$; (b) $Re = 10$.

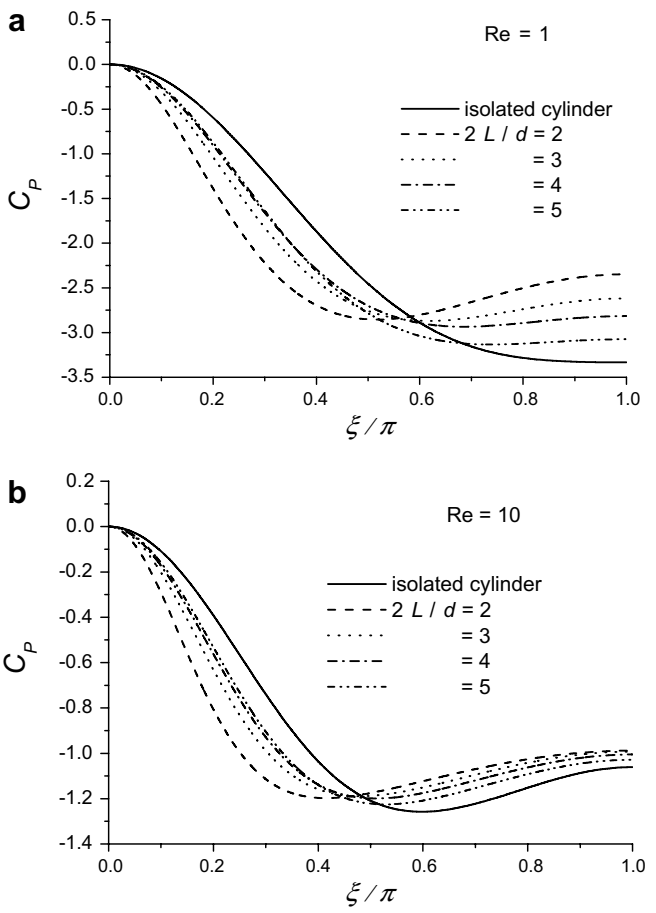

Fig. 8. The influence of the distance between cylinders on the surface pressure coefficient of the upstream cylinder; $d_1 = d_2 = d$; (a) $Re = 1$; (b) $Re = 10$.

problems usually discussed are the computation of the vorticity on the walls (the surface of the cylinders in our case) and the approximation of the derivatives $\partial\psi^*/\partial\xi, \partial\psi^*/\partial\eta$ (named here, for brevity, pseudo-velocities). The following relations were used to calculate the vorticity on the surface of the cylinders: Wilkes (Jensen) [40], Orszag and Israeli [40], Briley [40] and the compact relations presented by Spotz [41]. The pseudo-velocities were calculated numerically. The centered second-order scheme and the compact fourth-order scheme [21,24] were tested. We must mention that in the computation of the HOC discretization coefficients, the derivatives of

$$\frac{\bar{c}\sin\xi\sinh\eta}{(\cosh\eta-\cos\xi)^2} \quad \text{and} \quad \frac{\bar{c}(\cosh\eta\cos\xi-1)}{(\cosh\eta-\cos\xi)^2}$$

were calculated analytically.

One of the main problems in solving numerically the Navier–Stokes equations in unbounded regions is the boundary conditions at infinity. For the flow past an isolated cylinder, a reference article in solving this problem is [42]. In this case, i.e., the flow past an isolated cylinder, the free stream must be located at a large but finite distance from the cylinder center. For the present problem, in bipolar cylindrical coordinate system, the infinity of the physical space (x, y) is located in the point $\xi = \eta = 0$. For this reason, the boundary conditions (3b) were used in this work.

Only iterative methods were used to solve the discrete approximation of (7). Numerical experiments were made with different variants of point Gauss – Seidel and line Gauss – Seidel on grids with 33×33, 65×65, 129×129, 257×257 and 513×513 points. Also, the multigrid strategy developed by Kouatchou [43] was tested.

4. Results

The present mathematical model depends on three dimensionless parameters: Re, $2L_1/d_1$, and d_1/d_2. The values considered for the Reynolds number based on the diameter of the up-stream cylinder are $Re \leqslant 30$. For these values of the Re number, the laminar flow around an isolated circular cylinder has two hydrodynamic regimes:

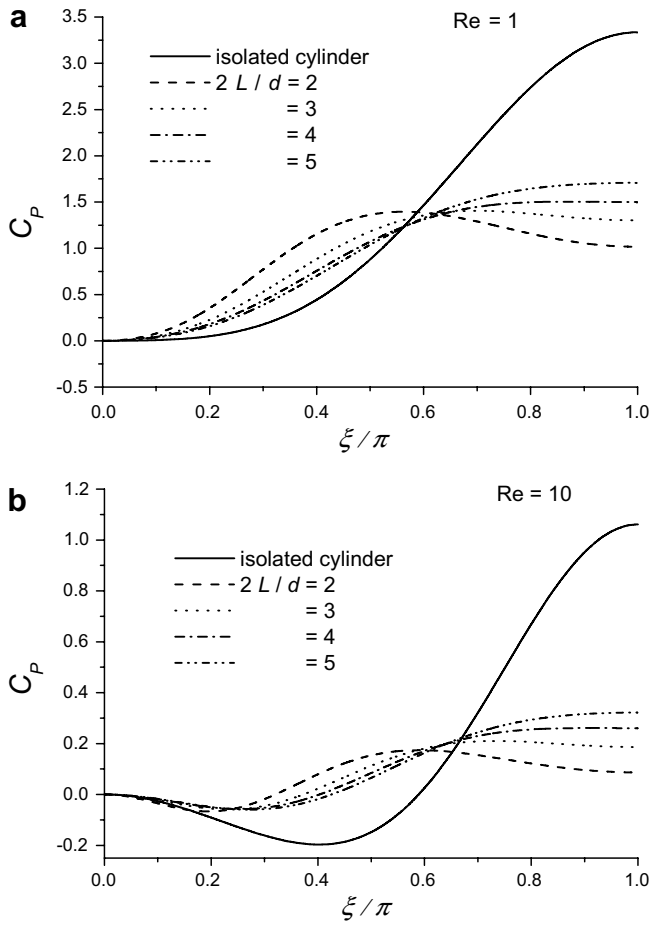

Fig. 9. The influence of the distance between cylinders on the surface pressure coefficient of the downstream cylinder; $d_1 = d_2 = d$; (a) $Re = 1$; (b) $Re = 10$.

steady flow without separation ($Re \leqslant 5$) and steady flow with two symmetric vortices behind the cylinder ($5 \leqslant Re \leqslant Re_{crt} \cong 46$). Numerical experiments were made with $2L_1/d_1$ taking values from 1.1 to 11 and $d_1/d_2 = 0.5, 1, 2$. Note that if $d_1 = d_2 = d$, it results in $L_1 = L_2 = L$.

The following aspects should be mentioned concerning the convergence of the iterative methods:

- for $2L_1/d_1 = 2$ and $d_1/d_2 = 0.5, 1, 2$, the numerical algorithms do not converge for $Re \leqslant 0.1$; at $Re = 0.2$ the convergence rate is very slow; under these conditions, we selected for presentation the results obtained at $1 \leqslant Re \leqslant 30$;
- for $d_1 = d_2 = d$ and $1 \leqslant Re \leqslant 30$, the iterative methods do not converge if $2L/d < 1.8$ and $2L/d > 5$;
- for $d_1/d_2 = 0.5, 2$, and $1 \leqslant Re \leqslant 30$, the numerical methods do not converge for $2L_1/d_1 > 2$.

For the driven cavity, at low Reynolds numbers, Gupta [21] showed that the relations used to calculate the wall vorticity and the velocities do not have a significant impact on the accuracy of the results. The accuracy criterion adopted for the present problem is the drag coefficient. Fig. 2 show that the numerical approximations of the pseudo-velocities do not influence practically the values of the drag coefficients on finer grids, where the solutions have the desired accuracy. The impact of the relations used to calculate the surface vorticity on the drag coefficients is negligible and does not deserve a distinct graphical presentation.

Table 1 summarizes the computations of the drag coefficients for $d_1 = d_2 = d$, $2L/d = 2$ (the gap between the cylinders is equal to the diameter of the cylinders) and $1 \leqslant Re \leqslant 30$. Fig. 3 shows the values of the drag ratios for the same parameters values (the drag ratio is defined as (drag coefficient for the tandem cylinder)/(drag coefficient for the isolated cylinder)). For $2L/d = 2$ and $d_1 = d_2 = d$, the influence of Re on the surface vorticity and surface pressure coefficient is plotted in Figs. 4 and 5, respectively. The influence of $2L/d$ on the drag ratio, surface vorticity and pressure coefficient is presented in Table 2 and Figs. 6–9, respectively. In Figs. 4–9, the surface's coordinate ξ/π varies from 0 to 1. For the upstream cylinder, the front stagnation point is located at $\xi/\pi = 0$ while the rear stagnation point at $\xi/\pi = 1$. For the downstream cylinder, the front stagnation point is located at $\xi/\pi = 1$ while the rear stagnation point at $\xi/\pi = 0$. Under these conditions, in each situation, the isolated cylinder data were adapted to be consistent with the present data. The results presented in Tables 1 and 2 and Figs. 3–9 were computed on a mesh with 513×513 points.

The results presented in Tables 1 and 2 and Figs. 3–9 lead to the following observations:

- the tandem interaction changes the surface vorticity and coefficient pressure for both cylinders; both cylinders experience a lower drag coefficient compared to the isolated cylinder; good agreement exists between the present results obtained at $Re = 1$ and those presented in [6];
- the surface vorticity and coefficient pressure on the front stagnation zone of the leading cylinder are not strongly influenced by the interaction; for the leading cylinder, the interaction's effects increase in the rear stagnation zone; flow separation occurs for $Re = 1$ at $2\ L/d < 3$;
- the strongest interaction effect is a radical change in the surface vorticity and coefficient pressure of the trailing cylinder; the wake of the leading cylinder exerts a strong influence on the trailing cylinder;
- the increase in Re decreases the interaction's effects for the upstream cylinder and amplifies these effects for the downstream cylinder;
- the increase in $2L/d$ from 2 to 5 decreases the interaction's effects.

For the steady, laminar flow past two spheres in-line, Tsuji et al. [44] showed that the tandem interactions are more pressure drag effects than friction drag effects. The

Table 3
Values of the drag coefficient for $d_1/d_2 \neq 1$ and 2 $L_1/d_1 = 2$

d_1/d_2	Re	C_{D1}	λ_1	C_{D2}	λ_2[a]
0.5	1	6.565	0.635	3.959	0.597
2		8.903	0.861	6.08	0.369
0.5	10	2.086	0.766	0.992	0.504
2		2.637	0.969	0.676	0.174

[a] Calculated using the C_D values for the isolated cylinder at $Re = 2$, 0.5, 20, 5.

interference effect of two objects placed in proximity in a stream flow can be analysed quantitatively in terms of drag coefficients. Fig. 3 shows that (a) for the leading cylinder, the pressure drag ratio is smaller than the friction drag ratio only for $Re < 15$; for $Re > 15$, the friction drag ratio is smaller than the pressure drag ratio; (b) for the trailing cylinder, the pressure drag ratio is smaller than the friction drag ratio for all Re values used in this work; the difference between the two drag ratios increases with the increase in Re. However, for both cylinders, we cannot state that one of the interaction's components (pressure or friction) is negligible in comparison with the other.

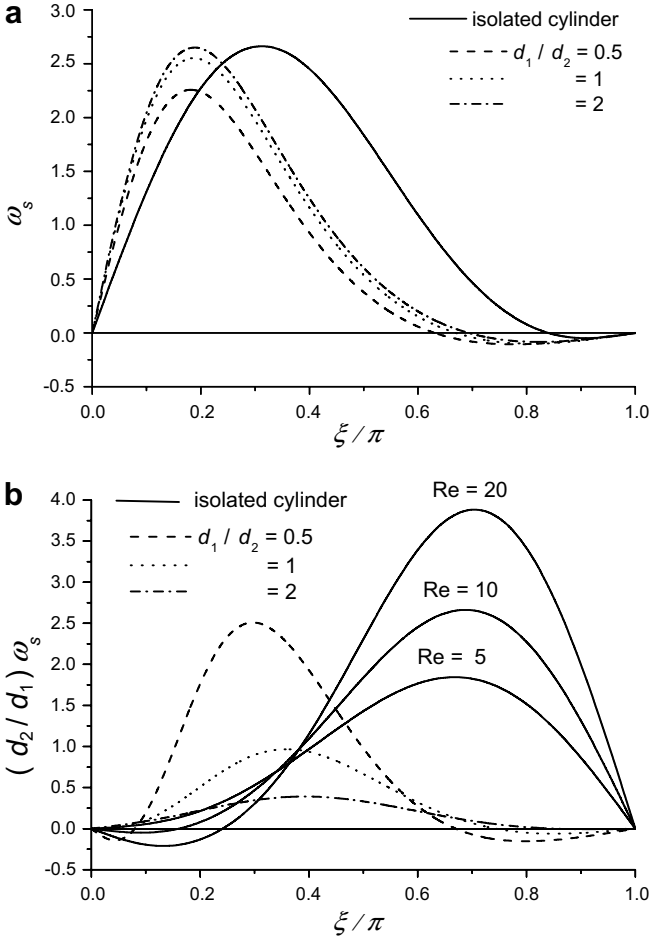

Fig. 10. The influence of the ratio of the cylinders diameters on the distribution of the vorticity over the surface of the cylinders; $Re = 10$; $2L_1/d_1 = 2$; (a) upstream cylinder; (b) downstream cylinder.

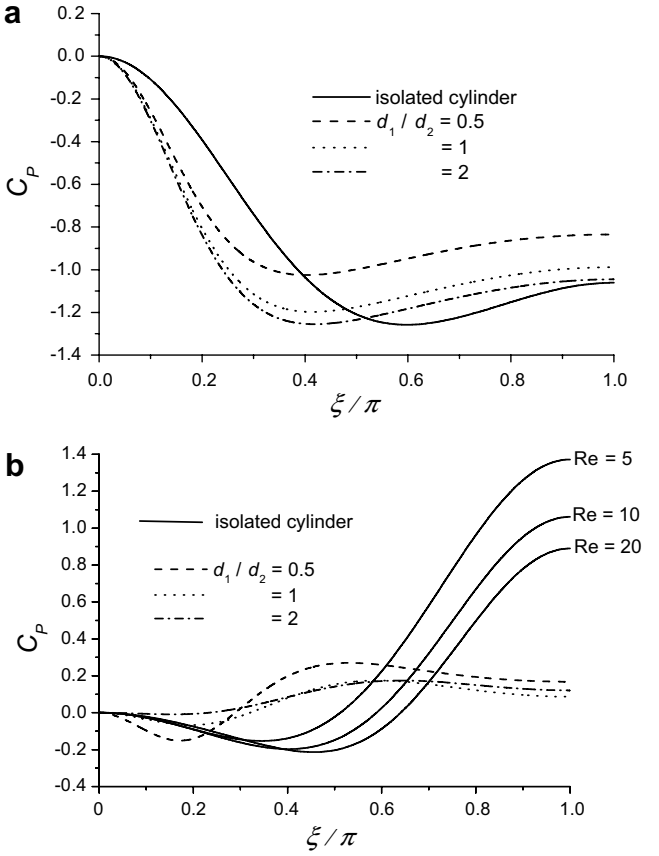

Fig. 11. The influence of the ratio of the cylinders diameters on the pressure coefficient over the surface of the cylinders; $Re = 10$; $2L_1/d_1 = 2$; (a) upstream cylinder; (b) downstream cylinder.

Experimental and numerical results obtained for two cylinders in tandem at $Re \geqslant 100$ show that the flow pattern abruptly changes when the spacing between the two cylinders is increased beyond a critical value (see [13] and the references mentioned herein). This critical value depends mostly on Re and lies in the range of [3.75, 4.0] diameters (this critical value is expressed as centre-to-centre distance) for Re in the range 100–200. For $Re \leqslant 30$, $d_1 = d_2$ and $2L/d$ in the range [2,5] we did not observe any discontinuity in the flow pattern. Table 2 and Figs. 6–9 show that the flow characteristics do not change significantly when $2L/d$ varies between 2 and 5.

Table 3 and Figs. 10 and 11 show that the tandem interaction's rules observed for $d_1 = d_2$ remain valid for $d_1 \neq d_2$. As expected, if $d_1 < d_2$ the deformation of the surface vorticity and coefficient pressure of the leading cylinder increase. However, even in this situation, the trailing cylinder remains the most affected by interaction. When $d_1 > d_2$, the interaction effects amplify significantly for the downstream cylinder while the changes undergone by the upstream cylinder are minor. In the analysis of the results obtained for $d_1 \neq d_2$, we considered the case $d_1 = d_2$ as comparison criterion.

5. Conclusions

We may summarize the numerical results obtained in this work as follows:

- the combination HOC finite difference schemes – iterative methods cannot solve the present problem for any combination of the parameters values;
- the interference effects are evidently greater on the trailing body than that on the leading body; these differences increase with the increase in *Re*;
- the drag of each individual body is smaller than the drag of the isolated body;
- the gap between the cylinders and the ratio of the diameters of the cylinders do not modify the main characteristics of the tandem interaction.

References

[1] M.M. Zdravkovich, Review of flow interference between two circular cylinders in various arrangements, ASME J. Fluids Eng. 99 (1977) 618–633.

[2] S.S. Chen, Flow – Induced Vibrations of Circular Cylindrical Structures, Hemisphere, New York, 1987.

[3] J. Li, A. Chambarel, M. Donneaud, R. Martin, Numerical study of laminar flow past one and two circular cylinders, Comput. Fluids 19 (1991) 155–170.

[4] A. Slaouti, P.K. Stansby, Flow around two circular cylinders by the random vortex method, J. Fluids Struct. 6 (1992) 641–670.

[5] S. Mittal, V. Kumar, A. Raghuvanshi, Unsteady incompressible flows past two cylinders in tandem and staggered arrangements, Int. J. Num. Meth. Fluids 25 (1997) 1315–1344.

[6] A.K.W. Cheung, B.T. Tan, K. Hourigan, M.C. Thompson, Interference drag between spherical and cylindrical particles in Stokes flow, in: 14th Australasian Fluid Mechanics Conference, Adelaide, Australia, 2001, pp. 115–118.

[7] J.R. Meneghini, F. Saltara, C.L.R. Siqueira, J.A. Ferrari Jr., Numerical simulation of flow interference between two circular cylinders in tandem and side-by-side arrangements, J. Fluids Struct. 15 (2001) 327–350.

[8] S. Mittal, V. Kumar, Flow-induced oscillations of two cylinders in tandem and staggered arrangements, J. Fluids Struct. 15 (2001) 717–736.

[9] B. Sharman, Numerical predictions of low Reynolds number flows over two tandem circular cylinders, Ph.D. Thesis, University of Waterloo, Ontario, Canada, 2002.

[10] B. Sharman, F.S. Lien, L. Davidson, C. Norberg, Numerical predictions of low Reynolds number flows over two tandem circular cylinders, Int. J. Numer. Meth. Fluids 47 (2005) 423–447.

[11] W. Jester, Y. Kallinderis, Numerical study of incompressible flow about fixed cylinder pairs, J. Fluids Struct. 17 (2003) 561–577.

[12] M.R. Khorrami, M.M. Choudhari, L.N. Jenkins, C.B. McGinley, Unsteady flow field around tandem cylinders as prototype for component interaction in airframe noise, in: 26th AIAA Aeroacoustics Conference, Monterey, California, 2005.

[13] J. Mizushima, N. Suehiro, Instability and transition of flow past two tandem circular cylinders, Phys. Fluids 17 (2005) 104107.

[14] Gh. Juncu, A numerical study of laminar flow past two circular cylinders in-line at low Reynolds numbers, Anal. Univ. Bucuresti, Seria Matematica LV, 2006, pp. 77–86.

[15] B.S. Carmo, Numerical investigation of the flow around two circular cylinders in tandem, Ph.D. Thesis, University of Sao Paolo, Sao Paolo, Brazil, 2005.

[16] D.L. Young, J.L. Huang, T.I. Eldho, Numerical simulation of high-Reynolds number flow around circular cylinders by a three-step FEM-BEM model, J. Eng. Mech. 121 (1995) 367–378.

[17] J.-L. Guermond, H.Z. Lu, A domain decomposition method for simulating advection dominated, external incompressible viscous flows, Comput. Fluids 29 (2000) 525–546.

[18] T. Farrant, M. Tan, W.G. Price, A cell boundary element method applied to laminar vortex shedding from circular cylinders, Comput. Fluids 30 (2001) 211–236.

[19] D. Russell, Z.J. Wang, A Cartesian grid method for modeling multiple moving objects in 2D incompressible viscous flow, J. Comput. Phys. 191 (2003) 177–205.

[20] S.C.R. Dennis, J.D. Hudson, Compact h^4 finite difference approximations to operators of Navier–Stokes type, J. Comput. Phys. 85 (1989) 390–416.

[21] M.M. Gupta, High Accuracy solutions of incompressible Navier–Stokes equations, J. Comput. Phys. 93 (1991) 343–359.

[22] I. Altas, K. Burrage, A high accuracy defect-correction multigrid method for incompressible Navier–Stokes equations, J. Comput. Phys. 114 (1994) 227–233.

[23] M. Li, T. Tang, B. Fornberg, A compact fourth-order finite difference scheme for the steady incompressible Navier–Stokes equations, Int. J. Numer. Meth. Fluids 20 (1995) 1137–1151.

[24] W.F. Spotz, G.F. Carey, High-order compact scheme for the steady stream-function vorticity equations, Int. J. Numer. Meth. Engng. 38 (1995) 3497–3512.

[25] E. Weinan, J.-G. Liu, Essentially compact schemes for unsteady incompressible flows, J. Comput. Phys. 124 (1996) 122–138.

[26] J. Zhang, Numerical simulation of 2D square driven cavity using fourth order compact finite difference schemes, Comput. Math. Appl. 43 (2003) 43–52.

[27] M. Ben-Artzi, J.-P. Croisille, D. Fishelov, S. Trachtenberg, A pure-compact scheme for the streamfunction formulation of Navier–Stokes equations, J. Comput. Phys. 205 (2005) 640–664.

[28] E. Erturk, C. Gökçöl, Fourth order compact formulation of Navier–Stokes equations and driven cavity flow at high Reynolds numbers, Int. J. Numer. Meth. Fluids 50 (2006) 421–436.

[29] J.-G. Liu, C. Wang, H. Johnston, A fourth order scheme for incompressible Boussinesq equations, J. Sci. Comput. 18 (2003) 253–285.

[30] J.-G. Liu, C. Wang, High order finite difference methods for unsteady incompressible flows in multi-connected domains, Comput. Fluids 33 (2004) 223–255.

[31] E.W. Weisstein, Bipolar cylindrical coordinates, MathWorld – A Wolfram web resource. http://mathworld.wolfram.com/BipolarCylindricalCoordinates.html.

[32] F.C. Thames, J.F. Thompson, C.W. Mastin, R.L. Walker, Numerical solutions for viscous and potential flow about arbitrary two-dimensional bodies using body-fitted coordinate systems, J. Comput. Phys. 24 (1977) 245–273.

[33] M.M. Gupta, R. Manohar, J.W. Stephenson, A single cell high order difference scheme for the convection diffusion equation with variable coefficients, Int. J. Numer. Meth. Fluids 4 (1984) 641–651.

[34] R. Manohar, J.W. Stephenson, High order difference scheme for linear partial differential equations, SIAM J. Sci. Stat. Comput. 5 (1984) 69–77.

[35] M.M. Gupta, R. Manohar, J.W. Stephenson, High-order difference schemes for two-dimensional elliptic equations. Numer, Meth. Partial Diff. Eqn. 1 (1985) 71–80.

[36] R.J. MacKinnon, G.F. Carey, Superconvergent derivatives: A Taylor series analysis, Int. J. Numer. Meth. Engng. 28 (1989) 489–509.

[37] R.J. MacKinnon, G.F. Carey, Nodal superconvergence and solution enhancement for a class of finite-element and finite-difference methods, SIAM J. Sci. Stat. Comput. 11 (1990) 343–353.

[38] W.F. Spotz, G.F. Carey, Formulation and experiments with high-order compact schemes for nonuniform grids, Int. J. Numer. Meth. Heat Fluid Flow 8 (1998) 288–303.

[39] J. Zhang, H. Sun, J.J. Zhao, High order compact schemes with multigrid local mesh refinement procedure for convection diffusion problems, Comput. Meth. Appl. Mech. Engng. 191 (2002) 4661–4674.

[40] E. Weinan, J-G. Liu, Vorticity boundary conditions and related issues for finite difference schemes, J. Comput. Phys. 124 (1996) 368–382.

[41] W.F. Spotz, Accuracy and performance of numerical wall boundary condition for steady, 2D, incompressible streamfunction vorticity, Int. J. Numer. Meth. Fluids 28 (1998) 737–757.

[42] B. Fornberg, A numerical study of steady viscous flow past a circular cylinder, J. Fluid Mech. 98 (1980) 819–855.

[43] J.R. Kouatchou Ngongang, High-order multigrid techniques for partial differential equations, Ph.D. Thesis, George Washington University, Washington DC, 1998.

[44] R. Tal (Thau), D.N. Lee, W.A. Sirignano, Heat and momentum transfer around a pair of spheres in viscous flow, Int. J. Heat Mass Transfer 27 (1984) 1953–1962.